Direct space representation of metallicity and structural stability in SiO solids

2002 J. Phys.: Condens. Matter 14 10251

(http://iopscience.iop.org/0953-8984/14/43/321)

INSTITUTE OF PHYSICS PUBLISHING JOURNAL OF PHYSICS: CONDENSED MATTER

J. Phys.: Condens. Matter **14** (2002) 10251–10263 PII: S0953-8984(02)38428-5

Direct space representation of metallicity and structural stability in SiO solids

Samantha Jenkins

Department of Informatics and Mathematics, University of Trollhättan/Uddevalla, PO Box 957, 461 29 Trollhättan, Sweden

E-mail: Samantha.Jenkins@htu.se

Received 20 June 2002
Published 18 October 2002
Online at stacks.iop.org/JPhysCM/14/10251

Abstract

First principles calculations are performed on possible structures of silicon monoxide solids. The chemical character of all of the bonding interactions is systematically quantified in real space. It is found that the most stable SiO structure possesses the highest number of inequivalent bond paths. This process reveals a novel metallic Si–Si interaction and provides an explanation for the origin of the unexpectedly high conductivity in thin silicon oxide layers. In this paper a new measure for quantifying metallic character (in direct space) present in a bond has been introduced. Furthermore it has been possible to determine the directional properties of this metallic character in real space using the charge density. This finding is very important for future complementary metal oxide semiconductor technology.

1. Introduction

As design of new materials on the atomic scale becomes more important, particularly in the field of nanotechnology, the use of more quantitative and local measures of chemical and physical properties becomes urgent. For instance, it is useful in a bulk situation to be able to calculate the binding energy, but this assumes an averaging of the bonding environments. At a surface, the simplest crystal becomes far more complex: there are now many more different bonding environments than in the bulk. Many of these bonds will be distorted and strained beyond of the reach of traditional chemical description. On surfaces there may well be various types of adatom or vacancy defect, which further complicate the bonding environment. Changes on a surface will have consequences further into the bulk, e.g. the commonly used technique of adding hydrogen atoms to passivate 'dangling' bonds. The ability to be able to follow these changes in the topology of the charge density in a quantitative and predictive manner is hence very important for surfaces, and also those changes produced by chemical reactions and the movement of defects and dislocations. For instance, it is possible to predict where a defect

will move from based on its instability at the site of the defect, and where it will move to as measured by the reactivity of the 'receptor' site [1].

The need for a quantum mechanical model that can quantitatively describe bonding locally, i.e. on a bond-by-bond basis, is clear. As far as this work is concerned the solids studied have a range of bonding environments including a solid that is a (2 + 1)-dimensional solid, an extended sheet structure. This model must provide both chemical and energetic descriptions to the bonding environment; the theory that has been used is the developing theory of 'atoms in molecules' AIM [2], sometimes called (somewhat unpronounceably) QTAIM, 'QT' standing for quantum theory.

The ability to obtain a detailed quantitative description on the little-studied monoxide system SiO is very important for the development of the complementary metal oxide semiconductor (CMOS) technology. This has enabled the understanding in particular of the origin of the unexpectedly high conductivity in thin silicon oxide layers.

In this paper a new measure for quantifying metallic character has been introduced, a simple relationship between the charge density and the Laplacian within the framework of the AIM theory. This relation was introduced to explore directly the relationship between the real space charge density distribution and the wealth of knowledge already in existence using the conventional reciprocal space based approach of solid-state physics. This approach could in the near future be used to describe how the electrical resistance of colossal magnetoresistive (CMR) materials [3] changes by orders of magnitude, effectively switching a material between insulating and metallic states. Band structures are calculated in reciprocal space, and in doing so the presence of metallic character and its variation with direction can be ascertained. If a substance shows metallic properties in reciprocal space it is reasonable to conclude that it may be possible to provide a real space description as well.

In this paper the results from *ab initio* electronic structure calculations are performed based on the five SiO structures postulated by Mankefors *et al* [4]. There exist no clear-cut experimental characterizations of bulk SiO, so it is important to relate any findings to previously known substances. This study refers to the familiar ideal tetragonal SnO-type structure [5] and its modifications as presented by Mankefors *et al* [4]. Five possible SiO structures were considered, comprising rocksalt, zincblende, wurtzite, the orthorhombically distorted SnO-type sheet structure and a hypothetical fivefold coordinated wurtzite structural analogue for reference. The superlattice calculations were performed in order to obtain the total electron density distributions for the five SiO structures and the SnO structure. The total electron density distributions are the entire basis for the work of this study. Readers are referred to [4] for diagrams of the rocksalt, zincblende and wurtzite structures; the fivefold coordinated wurtzite structural analogue and the orthorhombically distorted SnO type sheet structure are shown in figures 1 and 2 respectively. Relationships derived from the charge density are plotted and shown in figures 3 and 4. Point and directional properties of the bonding interactions are given in tables 1 and 2 respectively.

2. Method and computational details

All geometries for the different structural arrangements were calculated *ab initio*, using density functional theory (DFT) and employing the local density approximation as implemented by Ceperley and Alder [6] and Perdew and Zunger [7]. The calculations to obtain the correct atomic positions were performed using the plane-wave based code fhi94md.cth [8]. The theoretical lattice parameters of SiO were obtained from calculations performed by Mankefors *et al* [4] who also provided the relevant theoretical atomic positions [9]. The lattice parameters for SnO were taken from the work of Graeme W Watson [10] who also provided the theoretical atomic positions [11] using VASP [12–14] and the GGA.

Table 1. Variation of various quantities with BPL (bond path length in ångstroms (Å)), where $\rho(\boldsymbol{r}_b)$ and $H(\boldsymbol{r}_b)$ are given in atomic units (au), $|\lambda_1|/\lambda_3$, ε, $\xi(\boldsymbol{r}_b)$ and ELF are dimensionless and $De(\boldsymbol{r}_b)$ and $De_{\rm sum}(\boldsymbol{r}_b)$ are in electron volts (eV). The symbols are explained in the text.

SiO	BPL[a]	$\rho(\boldsymbol{r}_b)$	$\lvert\lambda_1\rvert/\lambda_3$	$\xi(\boldsymbol{r}_b)$	ε	$H(\boldsymbol{r}_b)$[b]	$De(\boldsymbol{r}_b)$	$De_{\rm sum}(\boldsymbol{r}_b)$	ELF[d]
				Relaxed SnO					
Si1–O3	1.786	0.099	0.180	0.205	0.003	−0.028	2.418	7.095[c]	0.141
Si1–O4	2.170	0.051	0.275	1.041	0.016	−0.021	0.730		0.273
Si1–Si2	2.962	0.034	0.480	5.667	0.168	−0.007	0.200		0.606
				Rocksalt					
Si1–O2	2.250	0.053	0.357	1.395	0.000	−0.017	0.602	3.614	0.388
				Tetragonal wurtzite analogue					
Si1–O4	1.618	0.140	0.147	0.126	0.000	−0.031	4.619	5.741	0.110
Si1–O3	2.618	0.030	0.264	0.732	0.014	−0.004	0.244		0.255
Si2–O4	2.882	0.018	0.192	0.474	0.000	−0.001	0.143		0.117
				Wurtzite					
Si2–O3	1.583	0.153	0.136	0.114	0.015	−0.034	5.495	5.999	0.103
Si1–O4	2.784	0.023	0.254	0.697	0.003	−0.002	0.168		0.202
				Zincblende					
Si1–O2	2.035	0.072	0.390	2.118	0.000	−0.033	1.028	4.111	0.415
				SnO relaxed					
Sn1–O3	2.246	0.064	0.193	0.288	0.015	−0.008	0.971	4.076	0.179
Sn1–Sn2	3.853	0.011	0.227	0.917	0.031	−0.0003	0.048		0.206

[a] The BPL was within 1% of the linear separations of bonded nuclei.
[b] $H(\boldsymbol{r}_b) = G(\boldsymbol{r}_b) + V(\boldsymbol{r}_b)$; $G(\boldsymbol{r}_b)$ and $V(\boldsymbol{r}_b)$ are the virial and the kinetic energy densities respectively.
[c] $De_{\rm sum}(\boldsymbol{r}_b) = 4 \times De(\boldsymbol{r}_b)_{\rm Si1-Si2} + 2 \times (De(\boldsymbol{r}_b)_{\rm Si1-O3} + De(\boldsymbol{r}_b)_{\rm Si1-O4}) = 7.095$ eV.
[d] The ELF values are evaluated at the BCP.

The total charge density distributions were obtained using CRYSTAL 98 [15]. Localized basis sets were used for the purposes of obtaining the total charge density distributions. For the silicon and oxygen atoms 6-31G* basis sets were initially selected, then diffuse functions were removed and the outer exponentials were carefully optimized in the SiO bulk using the code LOPTCG available within CRYSTAL98. The 6-31G* basis set is a so-called *split valence* set (single function for the core; two for the valence) with the core orbital of each atom described by a linear combination of six Gaussian primitives, and the two valence functions modelled respectively by (i) a linear combination of three Gaussians, and (ii) a lone (i.e., one) Gaussian primitive, the asterisk '*' denoting that a polarization function has been used.

For the Sn atoms the same optimization procedure was carried out on a general basis set, s(9), sp(7), sp(6), d(6), sp(3), sp(1), d(3), d(1), sp(1), sp(1), where the number in brackets refers to the number of primitive Gaussians for the particular shell.

Test calculations showed that the AIM theory was insensitive to the use of GGA or LDA. Analysis of the electron density to obtain the basic AIM properties was performed using TOPOND 98 [16].

3. Atoms in molecules (AIM)

The charge density $\rho(\boldsymbol{r})$ is a scalar field and its topological properties are reducible to a description of the number and type of its *critical points* (where $\boldsymbol{\nabla}\rho\ (\boldsymbol{r}_{\rm critical}) = 0$). These extrema in $\rho(\boldsymbol{r})$ can be characterized by the (3×3) matrix of second partial derivatives with

Table 2. The Cartesian components of the eigenvectors of the λ_1 and λ_2 eigenvalues. The eigenvectors of λ_2 show the direction of maximum metallic character, conversely the eigenvectors of the λ_1 show the direction of maximum insulating character. The relation $\lambda_1 \cdot \lambda_2 = 0$ holds for each M–O interaction, M = Si or Sn.

SiO	x	y	z
Relaxed SnO			
Si1–O3 λ_1	1.000	0.000	0.000
λ_2	0.000	0.572	−0.820
Si1–O4 λ_1	−0.529	0.000	0.849
λ_2	0.000	1.000	0.000
Si1–Si2 λ_1	−0.568	−0.010	−0.823
λ_2	0.482	−0.815	−0.323
Rocksalt			
Si1–O2 λ_1	0.000	1.000	0.000
λ_2	−1.000	0.000	0.000
Tetragonal wurzite analogue			
Si1–O4 λ_1	−0.001	−1.000	0.000
λ_2	−1.000	0.001	0.000
Si1–O3 λ_1	0.707	−0.707	0.000
λ_2	0.149	0.149	0.978
Si1–O4 λ_1	0.191	0.982	0.000
λ_2	−0.982	0.191	0.000
Wurtzite			
Si1–O4 λ_1	0.707	0.707	−0.008
λ_2	−0.707	0.707	0.000
Si1–O3 λ_1	−0.707	0.707	0.000
λ_2	−0.361	−0.361	−0.859
Zincblende			
Si1–O2 λ_1	−0.816	−0.408	−0.408
λ_2	0.000	−0.707	0.707
SnO (tetragonal structure)			
Relaxed			
Sn1–O4 λ_1	−1.000	0.000	0.000
λ_2	0.000	0.522	−0.853
Sn1–Sn2 λ_1	0.446	0.446	0.776
λ_2	0.707	−0.707	0.000

respect to coordinates of the charge density (the *Hessian* matrix), which when diagonalized, has four possible signatures (m, n), expressed as the number, m, of non-zero eigenvalues, and the arithmetic sum, n, of the signs of the eigenvalues (± 1).

The four possible sign patterns, (−1 −1 −1), (−1 −1 +1), (−1 +1 +1) and (+1 +1 +1), correspond to nuclear (3, −3), bond (3, −1), ring (3, +1) and cage (3, +3) critical points respectively. A (3, −3) maximum practically corresponds to a nucleus (more precisely there is a cusp in ρ at the nucleus). A ring critical point coincides with the bond critical point at the instant of a bond being ruptured. A (3, +3) minimum exists for example at the geometric centre of a C_{60} molecule. In this work only the bond critical points or BCPs (signature (3, −1)) are considered.

At a BCP, two curvatures are negative and ρ is a maximum at $\boldsymbol{r}_{\text{critical}}$ in the plane defined by their corresponding axes; ρ is a minimum at $\boldsymbol{r}_{\text{critical}}$ along the third axis, perpendicular to this plane. The existence of a BCP is a necessary condition for the formation of a bound state and implies the existence of an *atomic interaction line*—a line linking the nuclei along which

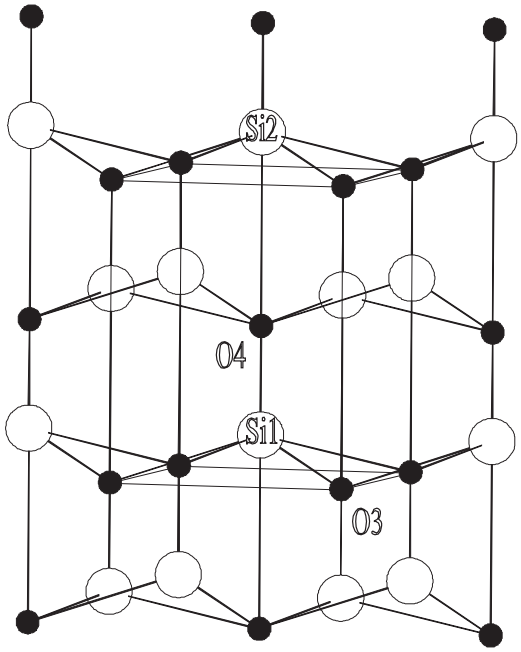

Figure 1. Tetragonal wurtzite analogue. The unit cell is outlined at the centre of the figure. Notice that the atoms are sixfold coordinated.

the charge density is a maximum with respect to any neighbouring line. If the forces resulting from the accumulation of electronic charge in the binding region are sufficient to exceed the anti-binding forces over a range of separations to yield an equilibrium configuration, then the state is bound and the atomic interaction line is called a *bond path*. The bond path usually coincides with the straight-line nuclear separation vector, but there are many exceptions to this which produce bond path lengths longer than the straight-line distance between nuclei. The molecular graph isolates the pairwise interactions present in the group of atoms, which dominate and characterize the properties of the system whether it is at equilibrium or in a state of change. The BCPs are found to join some but not all of the nuclear critical points. For instance, in the relaxed SnO-type structure for SiO there are BCPs between Si nuclei with a separation of 2.933 Å (bond path length of 2.962 Å) but there is *no* BCP between a pair of closer Si nuclei at 2.910 Å.

Critical points (BCPs for this work) may be further characterized by the (rotationally invariant) Laplacian of $\rho(\boldsymbol{r})$, $\nabla^2\rho(\boldsymbol{r})$, and by the principal axes and corresponding curvatures derived from the eigenvectors and corresponding ordered eigenvalues ($\lambda_1 < \lambda_2 < \lambda_3$) produced in the diagonalization of the Hessian of $\rho(\boldsymbol{r}_b)$, where the subscript b refers to a BCP. The eigenvalues λ_1 and λ_2 describe the plane perpendicular to the bond path which passes through the BCP, and the λ_3 eigenvector defines the direction of the bond path. Using AIM all interactions are characterized as one of two types, where there is a continuum of chemical character between the two types. These two types of interaction are designated according to the sign of the Laplacian of the charge density at the BCP, $\nabla^2\rho(\boldsymbol{r}_b)$: it is positive for a 'closed-shell' and negative for a 'shared-shell' interaction. Examples of the former are the strong 'covalent' carbon–carbon bonds in diamond [17], and those of the latter type include hydrogen bonds [18]. All of the bonding interactions in this study are of the closed-shell type.

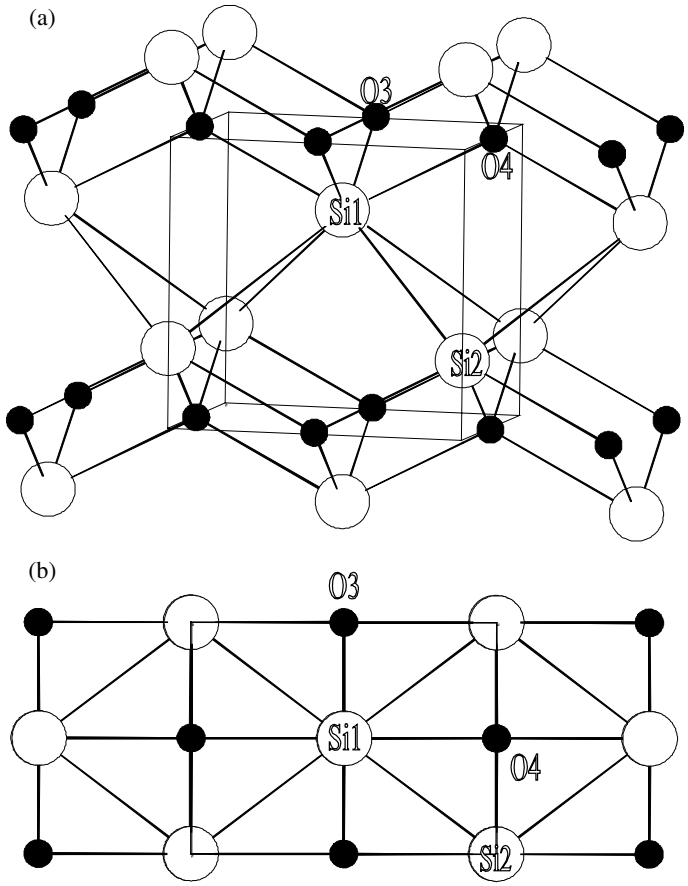

Figure 2. (a) Orthorhombically distorted SnO-type sheet structure viewed parallel to the ***ab*** plane. The unit cell is shown highlighted at the centre of the figure. (b) View of orthorhombically distorted SnO-type sheet structure parallel to the ***c***-axis.

The ellipticity is denoted by $\varepsilon = \lambda_1/\lambda_2 - 1$, and the eigenvectors associated with λ_2 and λ_1 provide a measure of the extent to which charge density is maximally and minimally accumulated respectively in a given plane locally perpendicular to the bond path. Large (e.g. >0.1) values of ellipticity also indicate π character as well as bond instability [19], and in such situations of large ellipticity the λ_2 eigenvector has previously been linked to the direction in which atoms most easily slide [20], and more recently the direction in which a defect hydrogen atom moves [1].

A degree of covalent character can be assigned [21, 22] to a bond for negative values of $H(\boldsymbol{r}_b)$, the total local energy density

$$H(\boldsymbol{r}_b) = G(\boldsymbol{r}_b) + V(\boldsymbol{r}_b)$$

where $G(\boldsymbol{r}_b)$ and $V(\boldsymbol{r}_b)$ are the local kinetic and virial energy densities respectively. All bonds investigated in this study satisfy this condition, though some only marginally as they have values of $H(\boldsymbol{r}_b)$ very close to zero. The dissociation energy per bond $De(\boldsymbol{r}_b)$ can be obtained from the atomic virial theorem [2] and is given by

$$De(\boldsymbol{r}_b) = -\tfrac{1}{2}V(\boldsymbol{r}_b).$$

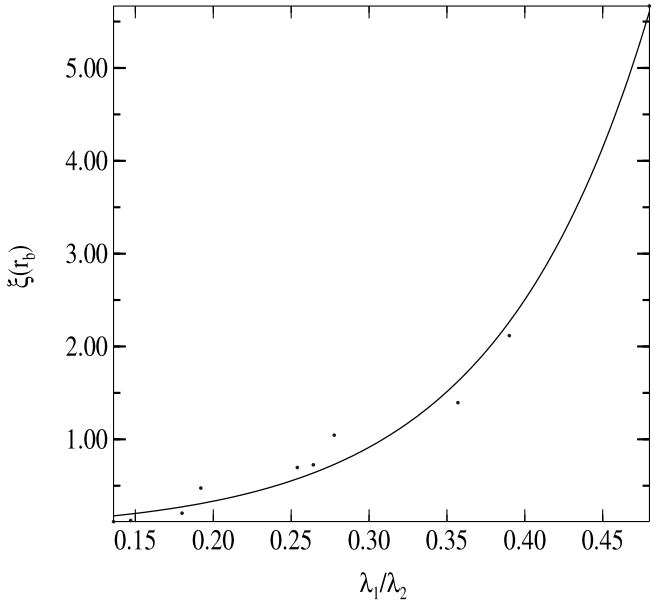

Figure 3. The relationship between the bond softness ($|\lambda_1|/\lambda_3$) and the 'metallicity' ($\xi(r_b)$) fits the simple exponential relation $\xi(r_b) = A\exp[B(|\lambda_1|/\lambda_3)]$ where $A = 0.044$ and $B = 10.077$ and the correlation was 0.995.

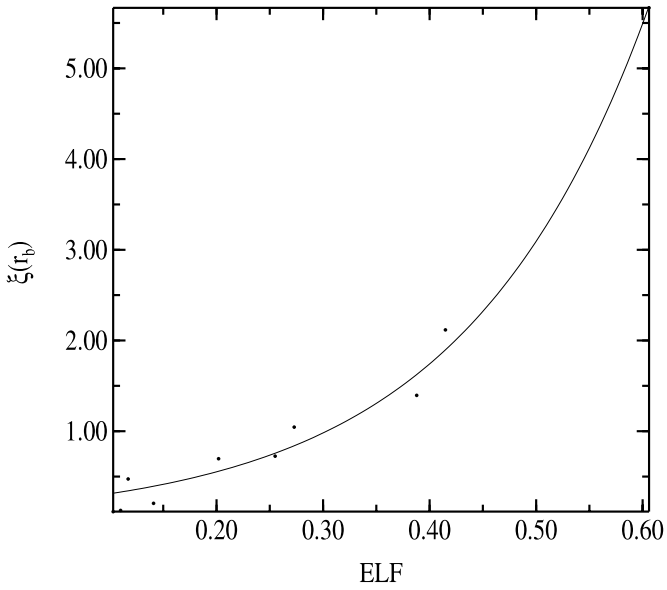

Figure 4. The relationship between the bond softness ELF (calculated at BCP) and the 'metallicity' ($\xi(r_b)$) fits the simple exponential relation $\xi(r_b) = A\exp[B(ELF)]$ where $A = 0.175$ and $B = 5.743$ and the correlation was 0.994.

This relation can be used to calculate the strength of all bonds in a structure on a bond-by-bond basis; its use was brought to light by the work of Espinosa *et al* [23]. It may be noticed that $V(r_b)$ and $De(r_b)$ are both energy densities, but since $V(r_b)$ is defined at a point (the BCP)

rather than over an area or volume the distinction between energy and energy density becomes unimportant for the purposes of obtaining the value of $De(\boldsymbol{r}_b)$. All the values of $De(\boldsymbol{r}_b)$ obtained in this paper and in a previous paper [1] were found to depend exponentially on the inter-nuclear separation d according to

$$De(\boldsymbol{r}_b) = A \exp[-Bd].$$

$De(\boldsymbol{r}_b)$ has this simple exponential dependence on inter-nuclear separation as $V(\boldsymbol{r}_b)$ is dependent on $\rho(\boldsymbol{r}_b)$, which is formed from the square of the (exponential) wavefunction. This is not a simple two-body interaction, as would be written in a simple inter-atomic potential; it is a relationship which holds for structures in mechanical equilibrium and only applies to two-body interactions when there is a BCP between the bodies. The latter criterion is many body and quantum mechanical in nature. For SiO the best-fit values of the constants are $A = 1613.9$ eV, $B = 3.606$ Å^{-1} and the correlation was 0.998.

Another quantity that shows the stability of a structure is the ratio of the largest negative eigenvalue and the positive eigenvalue at the BCPs, i.e. the ratio $|\lambda_1|/\lambda_3$. The larger the value of $|\lambda_1|/\lambda_3$ at a BCP, the 'softer' or fuzzier a bond is. This idea of bond softness is related to metallic character, so the softer a bond the more metallic it is. The inequality $|\lambda_1|/\lambda_3 < 1$ holds for all closed shell bonding interactions, and $|\lambda_1|/\lambda_3$ is related to the rigidity of the bond path. This can be seen from the fact that these interactions (all the bonding interactions in this paper are closed shell) are dominated by the contraction of charge away from the inter-atomic surface towards each of the respective atomic basins. The larger the value of $|\lambda_1|/\lambda_3$, the more the charge density remains at the BCP rather than moving towards the atomic basins, and the smaller the value of $\nabla^2\rho(\boldsymbol{r}_b)$ will be. This observation leads directly to the concept of metallicity; the Laplacian for closed shell interactions is always positive, a larger magnitude indicating a greater tendency for charge to move away from the BCP along the bond path into the two atomic basins connected by the bond path. A smaller value of the Laplacian means there is a greater tendency for the charge density to remain in the inter-nuclear region and away from atomic basins. This situation leads to bonding interactions with more metallic character. We can therefore define

$$\boldsymbol{\xi}(\boldsymbol{r}_b) = \rho(\boldsymbol{r}_b)/\nabla^2\rho(\boldsymbol{r}_b), \qquad \text{for } \nabla^2\rho(\boldsymbol{r}_b) > 0$$

where $\rho(\boldsymbol{r}_b)$ and $\nabla^2\rho(\boldsymbol{r}_b)$ are the values of the real space charge density and the Laplacian respectively at the BCP. This relation holds for $\nabla^2\rho(\boldsymbol{r}_b) > 0$, which is the case for metallic interactions. If the ratio $\xi(\boldsymbol{r}_b)$ is of the order of unity or less, then the BCP can be described as being non-metallic in character, or insulating. Values of $\rho(\boldsymbol{r}_b)$ and $\nabla^2\rho(\boldsymbol{r}_b)$ are listed in previous work, making it possible to calculate the metallicity (see table 7 in [1] under the heading interaction C4–C5, diamond). This is another example of a metallic bond, where for a metastable state (during kink-pair formation) in the unreconstructed core of the 90° partial in diamond, a closed shell C–C interaction has a $\xi(\boldsymbol{r}_b)$ of 3.30. This bond can be judged to be metallic, since it is responsible for the existence of a half-filled band. A description for metallic behaviour present in bonding interactions already exists within the formalism of the ELF (electron localization function) developed by [24] and is very elegant, since it describes all types of bonding by values of ELF (in the bonding region) between 0 and 1. In this paper the new simpler measure is introduced and can be used to compare the AIM based formalism for metallic versus insulating character. The reasoning behind this choice of relation to describe metallic character follows directly from the use of the bond 'softness' relation $|\lambda_1|/\lambda_3$. In figure 3 it can be seen that the bond softness $|\lambda_1|/\lambda_3$ is related to the metallicity $\xi(\boldsymbol{r}_b)$ by a simple exponential relation. The choice of $\xi(\boldsymbol{r}_b)$ fits with the intuitive idea of metallic behaviour; metallic character is associated with a low value of the charge density $\rho(\boldsymbol{r}_b)$ and

a slowly varying charge density. The variation in the charge density is associated with the second derivative of the charge density, the Laplacian.

In table 1 it can be seen that in the relaxed SnO-type structure, interlayer bonds exist and display metallicity at the BCP, as indicated by the large value of $\boldsymbol{\xi}(\boldsymbol{r}_b)$ and ELF value of 0.6, since an ELF value at the BCP of 0.5 indicates pure metallic bonding [25]. In figure 4 it can be seen that the value of ELF at the BCP is related to the metallicity $\xi(\boldsymbol{r}_b)$ by a simple exponential relation. Further to this, analysis of the properties derived from the charge density $\rho(\boldsymbol{r}_b)$ of these interlayer bonding interactions allows the direction of the metallic character to be deduced.

Since both charge and charge carrier accumulation and movement is preferential along the direction associated with λ_2 then the movement of charge and charge carriers will follow this direction too (see table 2 and [26]). Metallic properties follow from the movement of charge. Therefore if a bonding interaction is metallic, we can compare the Cartesian components of the eigenvector associated with λ_2 to the direction of maximum metallic character in real space. The maximum metallic character is effectively the minimum insulating character; conversely the Cartesian components of the eigenvector associated with λ_1 correspond to the direction of maximum insulating character and hence minimum metallic character. Where a bonding interaction has a zero value for the ellipticity, then the direction for the metallic character is still definable but there will not be a maximum in the metallicity in the direction associated with the λ_2 eigenvalue.

4. Results and discussion

4.1.1. Structural stability—energy comparison approach.

As an alternative to calculating the total energy of a particular structure as a means of comparing stabilities, an AIM based approach is used. This approach is beneficial for assessing relative structural stabilities as the contributions ($De(r_b)$ see table 1) to the total bond energy $De_{\mathrm{sum}}(r_b)$ arise only from the bonding.

The energy of all its bonded nearest neighbours to M is calculated as $De_{\mathrm{sum}}(r_b)$ in table 1 by summing the $De(r_b)$ values for each bond attached to a central Si or Sn. A larger value corresponds to a more stable structure. Immediately it is evident that the order of descending stability is SnO type structure, wurtzite, tetragonal wurtzite analogue, zincblende and rocksalt. The order of the wurtzite and tetragonal wurtzite with respect to stability is reversed compared with the work of Mankefors *et al* [4]. This is not surprising, as the pseudo-total energy has contributions other than those of the bonding interactions. But despite this difference there is still considerable agreement. In the SnO type structure the newly found Si–Si interaction (see figure 2) accounts for 11.3% of $De_{\mathrm{sum}}(r_b)$ (see table 1), and accounts for the most part for the increase in stability of the SnO relaxed structure over the next most stable structure, wurtzite. Each Si–Si bond is weak, with a $De(r_b)$ value of only 0.200 eV, but every Si has four such interactions to take into account and these four bonding interactions provide a greater contribution to $De_{\mathrm{sum}}(r_b)$ at 0.800 eV than does the Si1–O4 bonding interaction which provides 0.730 eV.

4.1.2. Structural stability—bonding network approach.

Examination of the bonding network (molecular graph) of the five given structures shows an evolution from the rocksalt structure through to the relaxed SnO structure—in order of decreasing isotropic character: rocksalt, zincblende, wurtzite tetragonal wurtzite and relaxed

SnO structure. Use of space group operators provides a simple way to state the relative degree of isotropic character present in these structures, but the use of AIM analysis of the relaxed charge densities of the five given structures allows a deeper understanding of the nature of the evolution of the structures than can be provided by the symmetry alone, and so is used in this study. AIM analysis of the relaxed charge densities of the rocksalt, zincblende and wurtzite structures produced no new bond paths that would not be considered with a purely valence driven model of bonding.

The rocksalt and zincblende structures are the most isotropic; they have only one inequivalent bond path per unit cell and the BCPs possess very small values of ε, of order 1×10^{-16} (see table 1). In the structures (rocksalt and zincblende) with only one inequivalent bond path per unit cell the silicon and oxygen nuclei are everywhere fourfold coordinated. The wurtzite structure contains two inequivalent bonds which both possess non-negligible values of ε (see table 1), which can be explained by the wurtzite having a hexagonal unit cell. The Si–O basal bonds are more unstable than the Si–O bonds parallel to the c axis (labelled Si1–O4 in table 1); this is indicated by the value of ε being an order of magnitude lower than for the Si–O bonds parallel to the c-axis. The wurtzite structure is everywhere fourfold coordinated. The tetragonal wurtzite structure was found to be sixfold coordinated (see figure 1), the sixth bond being Si2–O4, with three inequivalent bond paths, demonstrating a wider bonding environment than the wurtzite structure. The basal bonds were found to be weaker and less stable (larger values of ε) than the c-axis bonds (labelled Si1–O4 in table 1), as was found to be the case for the wurtzite structure. The SnO-type relaxed structure was found to have three inequivalent bond path lengths, with eight bond paths emanating from each silicon nucleus.

To summarize then, the number of inequivalent bond paths increases from one to three whilst the connectivity increases from fourfold to eightfold, from the rocksalt through to the relaxed SnO-type structure. Notice that although the tetragonal structure has the same number of inequivalent bond paths as does the SnO-type relaxed structure, the latter structure possesses the higher values of ε. These results are in agreement with those of [4] since they predict the same order of increasing stability from the rocksalt to the relaxed SnO-type structure.

4.2.1. Chemical character of M–O bonding interactions—covalency and ionicity.

From table 1 it can be seen for all five structures considered in this study, namely rocksalt, tetragonal wurtzite, wurtzite, zincblende and relaxed SnO-type structures, that all of the interactions are closed shell for both SiO and SnO (since $\nabla^2\rho(\boldsymbol{r}_b) > 0$). This means that all of the interactions have some degree of ionic, or rather polar-ionic character. Any further chemical characteristics of bonding interactions, such as covalent character and metallic character are found in the structures studied to vary from very substantial to negligible. The most stable structures have the broadest range of bonding character, quantified by the values of the bond softness $|\lambda_1|/\lambda_3$, the newly defined indicator of electrical character $\xi(\boldsymbol{r}_b)$, ellipticity ε and $H(\boldsymbol{r}_b)$.

The high symmetry rocksalt and zincblende structures both possess values of ellipticity $\varepsilon = 0$ for the single inequivalent bonding interactions. It has already been observed that zero values of ellipticity are indicative of sp^3 hybridization [1]. The dominance of the electrostatic energy contribution is shown by the small values of $\xi(\boldsymbol{r}_b)$ (which corresponds to a relatively large value of $\nabla^2\rho(\boldsymbol{r}_b)$) and a low value of $H(\boldsymbol{r}_b)$.

The low value of $\xi(\boldsymbol{r}_b)$ in the zincblende structure shows a much better balance of the electrostatic and covalent contributions to the lattice energy. The covalent contribution to the lattice energy for the zincblende structure is more than twice that of the rocksalt structure, indicated by the magnitude of $H(\boldsymbol{r}_b)$. The wurtzite structure achieves a better balance between

ionic and covalent than do the rocksalt or zincblende structures; this is seen from the range of values of $\xi(\boldsymbol{r}_b)$ and $H(\boldsymbol{r}_b)$ in table 1. The tetragonal wurtzite analogue achieves a better mix of ionicity/covalency still, and the best overall mix of ionicity/covalency of all five structures in this study is found in the SnO-type relaxed structure, as can be seen from the widest range of values of $\xi(\boldsymbol{r}_b)$ and $H(\boldsymbol{r}_b)$ in table 1.

4.2.2. Chemical character of M–O bonding interactions—metallicity.

Mankefors *et al* [4] noticed that superimposed on the expected semiconductor-like gap between the occupied 'bonding' and unoccupied 'anti-bonding' valence bands was found a non-negligible density of states at the Fermi level of SiO in the SnO-type relaxed structure. Metallic character in this work is characterized by a value of $\xi(\boldsymbol{r}_b) > 1$ or more, and found for the Si1–Si2 interaction in the SiO orthorhombically distorted SnO-type structure, but not in the tetragonal wurtzite analogue or in the SnO-type structure. Values of $\xi(\boldsymbol{r}_b)$ close to 1 denote semi-metallic character, and values less than 0.6 denote insulating character. It was also pointed out by Mankefors *et al* that the metallic signature was due the dominance of the Si PDOS at the Fermi level, suggesting that it is indeed the increase in Si–Si overlap which is responsible for this metallic property. Of course this increased Si–Si overlap leads to the existence of a Si–Si bonding interaction.

Using quantities derived using AIM one is able to provide quantitative explanations for the observations regarding metallicity made by Mankefors and co-workers. Simply stated: the Si–Si bonding interaction found in the orthorhombically distorted SnO-type structure is responsible for the observed metallic behaviour. The dominance of the metallic character in the Γ–Y direction in reciprocal space (parallel to the $\boldsymbol{b}$ direction in real space) is found to be in agreement with the results of table 2. The non-negligible value of $\xi(\boldsymbol{r}_b)$ (see table 1) for the Si1–O4 interaction can be explained by the metallic character of the Si1–Si2 bonding interaction 'leaking' into the Si1–O4 bond. The idea that bonds can leak their character into one another is not new: in the 1930s Pauling thought that the unusual properties of normal ice (e.g. expanding upon cooling below 4 °C) were due to the hydrogen bonds possessing a small admixture of the bonding characteristics of the covalent bonds [27]; later experimental [28] and theoretical work [22] confirmed this. The mixing of bonding character in the Si1–O4 interaction can be explained by the dominance of the metallic bonding in the y direction in the Si1–Si2 bonding interaction and the fact that the eigenvector of the λ_2 eigenvalue for the Si1–O4 lies parallel to the y-axis (see table 2). The metallic Si1–Si2 bonding interaction contains a degree of covalent character; this was the description given by Pauling [27] and more recently Silvi and Gatti [29]. Importantly for the AIM study of metals and metallicity, Silvi and Gatti found that the existence of a non-nuclear attractor of the electron charge density gradient field was not a prerequisite for metallic behaviour.

5. Conclusions

Although this investigation has used a different approach than was used in [4], agreement has been largely achieved. The presence of the non-negligible density of states at the Fermi level of SiO in the orthorhombically distorted SnO-type structure is manifested in this work by the presence of Si–Si bonding interactions. The metallic character found mainly along the $\boldsymbol{b}$ (Γ–Y) direction correlated very well with the eigenvector of the λ_2 eigenvalue of the Si–Si bonding interaction. The lack of strong metallic character in both the tetragonal SiO and relaxed SnO structures was also illustrated by the lack of dominance of the $\boldsymbol{b}$ direction of the λ_2 eigenvalue, again in agreement with this previous work. The origin of the unexpectedly

high conductivity in thin silicon oxide layers can be explained by the presence of the newly found metallic interactions (Si1–Si2) found connecting the layers of the SnO type relaxed SiO structure. From this work the hypothesis is drawn that the presence of metallic band structures indicates the presence of a bonding interaction, even when a bond is not suspected of being present.

Future work will concentrate on applying these extensions of the AIM theory to other such technologically important and interesting systems including those possessing CMR, such as manganate perovskite materials based on $LaMnO_3$. The introduction of the ratio $\xi(\boldsymbol{r}_b)$ will be the subject of further work on a range of suspected metallic, semi-metallic and insulating compounds to deepen the understanding of the real space approach to metallicity. Also investigations will be undertaken to test the hypothesis that the presence of metallic band structures indicates the presence of a bonding interaction, especially in cases where no known instances of bonding exist, as was the case for the SnO-type structure prior to this study.

Acknowledgments

Thanks are given to Stefan Mankefors and Graeme W. Watson for their assistance in obtaining the relaxed starting geometries for the SiO and SnO structures respectively. Thanks are also given to Joe Muscat, Ian Bytheway and Mike Towler (re CRYSTAL basis sets), and to Steven R Kirk for proof reading this manuscript. Thanks also to Malcolm Heggie for helpful discussions regarding the band structure of the unreconstructed core of the 90° partial in diamond. Thanks are also given to Enrique Espinosa and Bernard Silvi for discussions on AIM and ELF respectively.

Acknowledgement is given to Sherbrooke University (Canada) parallel computing facilities for computing support.

References

[1] Jenkins S and Heggie M I 2000 *J. Phys.: Condens. Matter* **12** 10325–33
[2] Bader R F W 1998 *Atoms in Molecules: a Quantum Theory (The International Series of Mongraphs on Chemistry vol 22)* (Oxford: Oxford University Press)
[3] Salamon M B, Lin P and Chun S H 2002 *Phys. Rev. Lett.* **88** 197203
[4] Mankefors S, Andersson T G and Panas I 2000 *Chem. Phys. Lett.* **322** 166–74
[5] Pannetier J and Denes G 1980 *Acta. Crystallogr.* B **36** 2736
[6] Ceperley D M and Alder B J 1980 *Phys. Rev. Lett.* **45** 566
[7] Perdew J P and Zunger A 1981 *Phys. Rev.* B **23** 5048
[8] Stumpf R and Scheffler M 1994 *Comput. Phys. Commun.* **79** 447
[9] Mankefors S 2001 private communication
[10] Watson G W 2001 *J. Chem. Phys.* **114** 758–63
[11] Watson G W 2001 private communication
[12] Kresse G and Hafner J 1994 *Phys. Rev.* B **49** 14251
[13] Kresse G and Furthmüller J 1996 *Comput. Mater. Sci.* **6** 15
[14] Kresse G and Furthmüller J 1996 *Phys. Rev.* B **54** 11169
[15] Saunders V R, Dovesi R, Roetti C, Causà M, Harrison N M, Orlando R and Zicovich-Wilson C M 1998 *CRYSTAL98 User's Manual* University of Torino
[16] Gatti C 1999 *TOPOND 98 User's Manual* CNR-CSRSRC Milano
[17] Abramov Y U A and Okamura F P 1997 *Acta Crystallogr.* A **53** 187–98
[18] Jenkins S and Morrison I 1999 *J. Chem. Phys.* **103** 11041
[19] Koch U and Popelier P L A 1995 *J. Chem. Phys.* **99** 9747
[20] Bone R G A and Bader R F W 1996 *J. Chem. Phys.* **100** 10892
[21] Cremer D and Kraka E 1984 *Croatica Chem. Acta* **57** 1250
[22] Jenkins S and Morrison I 2000 *Chem. Phys. Lett.* **317** 97
[23] Espinosa E, Molins E and Lecomte C 1998 *Chem. Phys. Lett.* **285** 170

[24] Silvi B and Savin A 1994 *Nature* **371** 683
[25] Peressi M, Fornari M, Gironcoli S D E, Santis L D E and Baldereschi A 2000 *Phil. Mag.* B **80** 515–21
[26] Jenkins S 1999 *PhD Thesis* Salford University
[27] Pauling L 1948 *The Nature of the Chemical Bond* (Ithaca, NY: Cornell University Press)
[28] Isaacs E D, Shukla A, Platzman P M, Hamann D R, Barbiellini B and Tulk C A 1999 *Phys. Rev. Lett.* **82** 600
[29] Silvi B and Gatti C 2000 *J. Chem. Phys.* **104** 947–53